

Supporting Information

Li₂CuPS₄ Superionic Conductor: A New Sulfide-Based Solid-State Electrolyte

Zhenming Xu, Ronghan Chen, Hong Zhu*

*University of Michigan–Shanghai Jiao Tong University Joint Institute,
Shanghai Jiao Tong University, Shanghai, 200240, China*

*Corresponding author:
E-mail: hong.zhu@sjtu.edu.cn

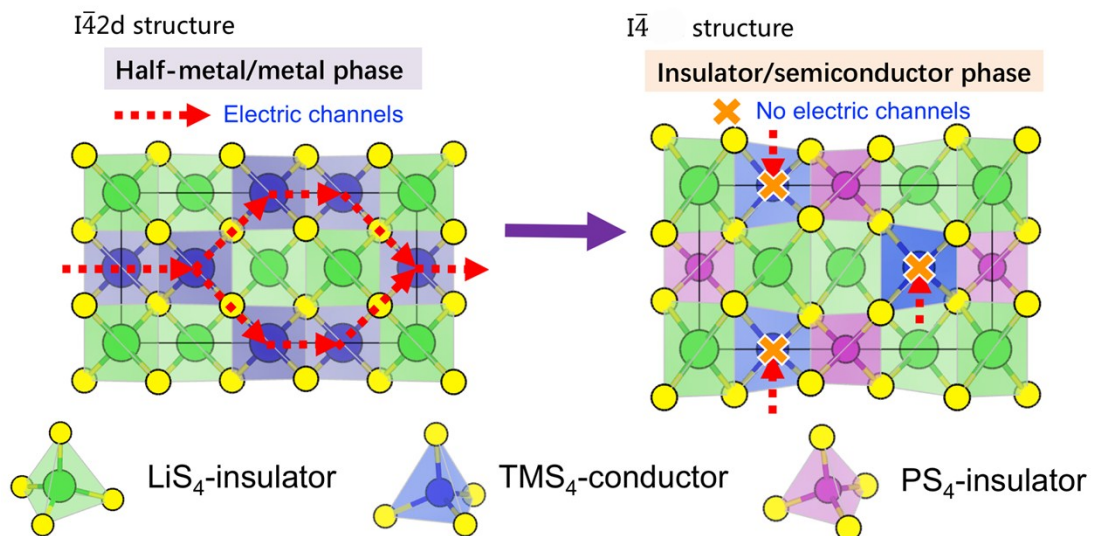


Figure S1. The logic flow of proposing the insulting $\bar{I}^4\text{-Li}_2\text{CuPS}_4$ from the metallic $\bar{I}^4\text{2d-LiMS}_2$ ¹ by introducing the insulting PS_4 tetrahedron to block electronic transport channel and considering the small electronegativity difference between P and S element.

Table S1. Three different phase structures (like $\text{Cu}_2\text{ZnSnS}_4$ ²) with the same Li_2CuPS_4 formula and their relative energies (in meV/atom).

Structure type	kesterite	stannite	primitive mixed CuAu-like
Space group	\bar{I}^4	$\bar{I}^4\text{2m}$	$\text{P}\bar{4}2m$
Relative energy	0	28	61

Table S2. Lattice constants and atomic coordinates of I⁴-Li₂CuPS₄ unit cell

	<i>a</i> /Å	<i>b</i> /Å	<i>c</i> /Å
	5.54079	5.54079	9.89418
	α	β	γ
	90°	90°	90°
	<i>x</i>	<i>y</i>	<i>z</i>
Li1	0	0	0
Li2	0.5	0.5	0.5
Li3	0.5	0	0.25
Li4	0	0.5	0.75
Cu1	0.5	0	0.75
Cu2	0	0.5	0.25
P1	0	0	0.5
P2	0.5	0.5	0
S1	0.275126	0.708064	0.120446
S2	0.724874	0.291936	0.120446
S3	0.708064	0.724874	0.879554
S4	0.291936	0.275126	0.879554
S5	0.775126	0.208064	0.620446
S6	0.224874	0.791936	0.620446
S7	0.208064	0.224874	0.379554
S8	0.791936	0.775126	0.379554

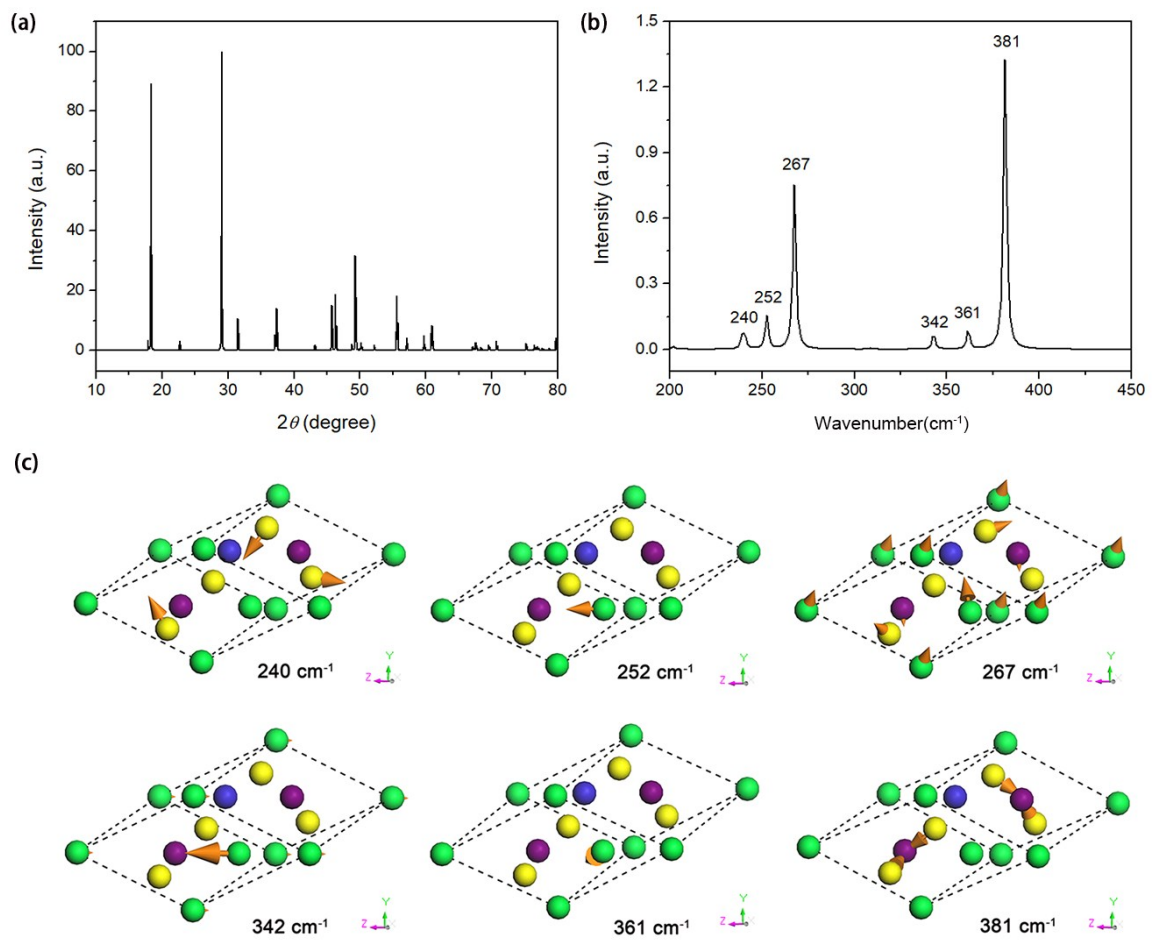


Figure S2. Simulated structural characterizations of $\bar{\text{I}}^4\text{-Li}_2\text{CuPS}_4$. (a) X-ray diffraction (XRD) pattern, (b) Raman spectrum with six major activation modes and (c) the corresponding vibrational structures of unit cell. Orange arrows represent the directions of vibration. Here, green, blue, purple and yellow balls denote Li atoms, Cu atoms, P atoms and S atoms., respectively.

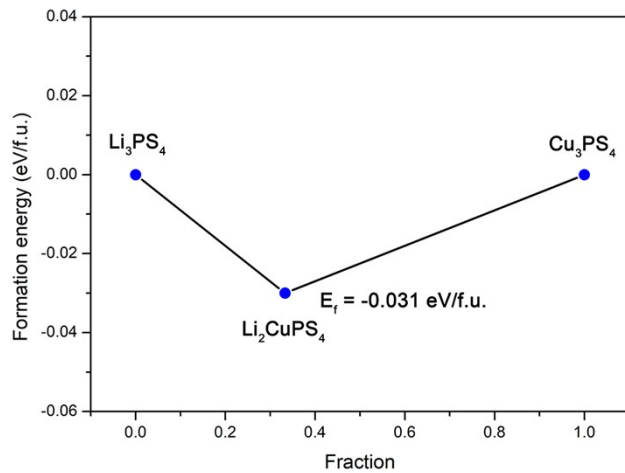


Figure S3. DFT calculated formation energy of Li_2CuPS_4 from its phase equilibria compounds of Li_3PS_4 and Cu_3PS_4 .

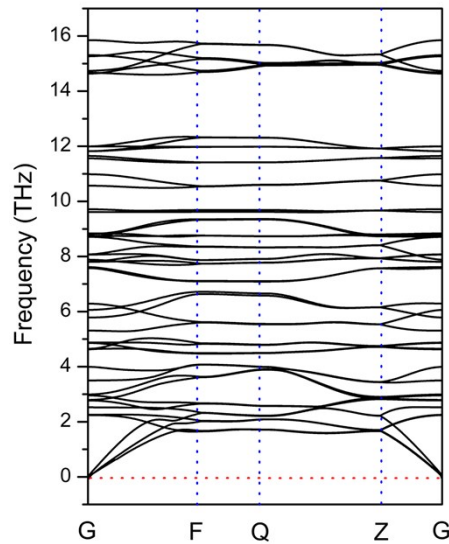


Figure S4. Phonon dispersion spectrum of the ground-state Li_2CuPS_4 .

Table S3. Calculated elastic constants (in GPa), Bulk modulus (B , in GPa), Young's modulus (E , in GPa), Shear modulus (G , in GPa) and B/G under the Reuss scheme of lithium metal³, Li_3PS_4 ⁴ and Li_2CuPS_4 material

	C_{11}	C_{12}	C_{13}	C_{22}	C_{23}	C_{33}	C_{44}	C_{55}	C_{16}	C_{66}	B	E	G	B/G
Li	14.60	13.80	-	-	-	-	11.5	-	-	-	13.92	6.26	2.20	6.32
$\beta\text{-Li}_3\text{PS}_4$	47.82	15.93	17.90	36.23	10.20	28.46	12.88	9.81		12.17	20.50	28.90	11.13	1.89
$\gamma\text{-Li}_3\text{PS}_4$	44.19	25.60	22.20	50.10	20.64	56.50	13.24	16.11	-	14.78	31.84	36.88	13.90	2.26
Li_2CuPS_4	68.95	28.45	38.29	-	-	60.12	34.97	-	0.60	26.12	45.34	54.60	21.01	2.16

Table S4. Space groups and IDs of the DFT ground state crystal structures in Materials Project (MP) database for the quaternary and pseudo-binary phase diagram calculations (Figure 1 and S2) of Li_2CuPS_4 .

Material	Space group	ID in MP database	Material	Space group	ID in MP database
Li	$\text{Im}\bar{3}\text{m}$	mp-135	Cu_2P_7	$\text{C}2/\text{m}$	mp-28034
LiCu_3	$\text{I}4/\text{mmm}$	mp-862658	CuS_2	Pnnm	mp-849086
Li_2CuP	$\text{P}6_3/\text{mmc}$	mp-12029	CuS	Cmcm	mp-555599
$\text{Li}(\text{CuP})_2$	$\text{I}4/\text{mmm}$	mp-7298	Cu_7S_4	Pnma	mp-624299
$\text{Li}_5(\text{Cu}_2\text{P}_3)_2$	Immm	mp-865734	CuPS_3	$\text{P}4_2/\text{mnmm}$	mp-1105187
LiP	$\text{P}2_1/\text{c}$	mp-9588	Cu_3PS_4	$\text{Pmn}2_1$	mp-3934
Li_3P	$\text{P}6_3/\text{mmc}$	mp-736	P	$\text{P}2/\text{c}$	mp-568348
LiP_7	$\text{I}4_1/\text{acd}$	mp-27687	P_2S_7	$\text{P}\bar{1}$	mp-1006118
Li_3P_7	$\text{P}2_1\text{I}2_1$	mp-28336	P_2S_5	$\text{P}\bar{1}$	mp-541788
Li_3PS_4	Pnma	mp-985583	P_4S_9	$\text{P}2_1/\text{c}$	mp-542630
LiS_4	P1	mp-995393	P_4S_7	$\text{P}2_1/\text{c}$	mp-2650
Li_2S	$\text{Fm}\bar{3}\text{m}$	mp-1153	P_4S_3	Pnma	mp-1468
Cu	$\text{Fm}\bar{3}\text{m}$	mp-30	S	$\text{P}2/\text{c}$	mp-96
CuP_2	$\text{P}2_1/\text{c}$	mp-927	Li_2CuPS_4	$\text{I}\bar{4}$	This work
CuP_{10}	P1	mp-606644			

Defect calculations

In this work, we considered three types of lithium point defects in LCPS based on the $2\times2\times1$ supercell models, including neutral and charged Li vacancy (V_{Li} and V_{Li}^-), neutral and charged interstitial Li (Li_i and Li_i^+ , both at the tetrahedral and octahedral center interstitial sites), and Li Frenkel vacancy-interstitial pairs (Li_{Fr} , both at the tetrahedral and octahedral center interstitial sites) (following Figure S4). We found Li site-1 is approximatively equal to the Li site-2 in terms of energy. Thus, we only focused on a Li vacancy site in this work. Formation energies of defect i at charge state q were calculated by^{5,6}

$$E_f(i, q) = E_{\text{tot}}(i, q) - E_{\text{tot}}(\text{bulk}) - n_{Li}\mu_{Li} + q(\varepsilon_F + E_{VBM}) + E_{\text{correct}}$$

where $E_{\text{tot}}(i, q)$ and E_{tot} (perfect bulk) are the total energies of defective and pristine LCPS supercell, respectively. The number of Li atoms (ions) added to ($n_{Li} > 0$) or removed from ($n_{Li} < 0$) the perfect supercell is n_{Li} , and μ_{Li} is the chemical potential of Li, which is referenced to the bulk energy of Li metal. Note that ε_F , which is defined relative to the valence-band maximum (E_{VBM}) of the perfect LCPS. E_{correct} is the corrected electrostatic interaction between the defect and its periodic images⁷.

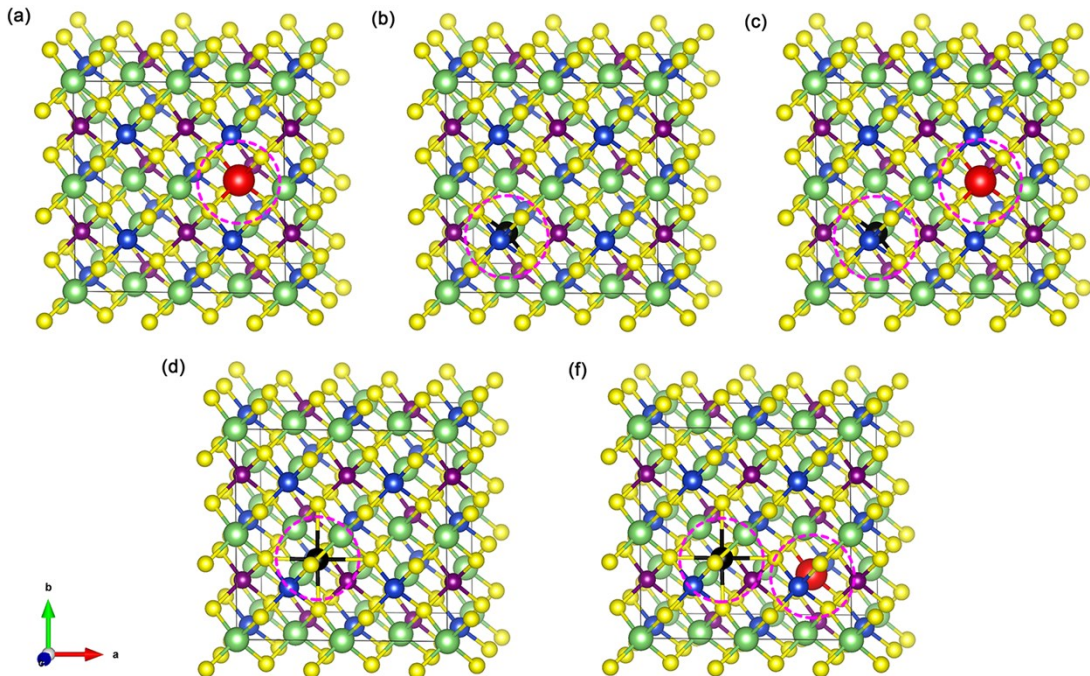


Figure S5. Defective structure models of (a) Li vacancy, (b) Li interstitial (tetrahedron center interstitial site), (c) Li Frenkel vacancy-interstitial (tetrahedron center interstitial site) pair, (d) Li interstitial (octahedron center interstitial site) and (e) Li Frenkel vacancy-interstitial (octahedron center interstitial site) pair in $2\times2\times1$ supercell of LCPS. Here, green, blue, purple, yellow, black and red balls denote Li atoms, Cu atoms, P atoms, S atoms, Li interstitial and Li vacancy atoms, respectively. The structure diagrams were displayed by VESTA code⁸.

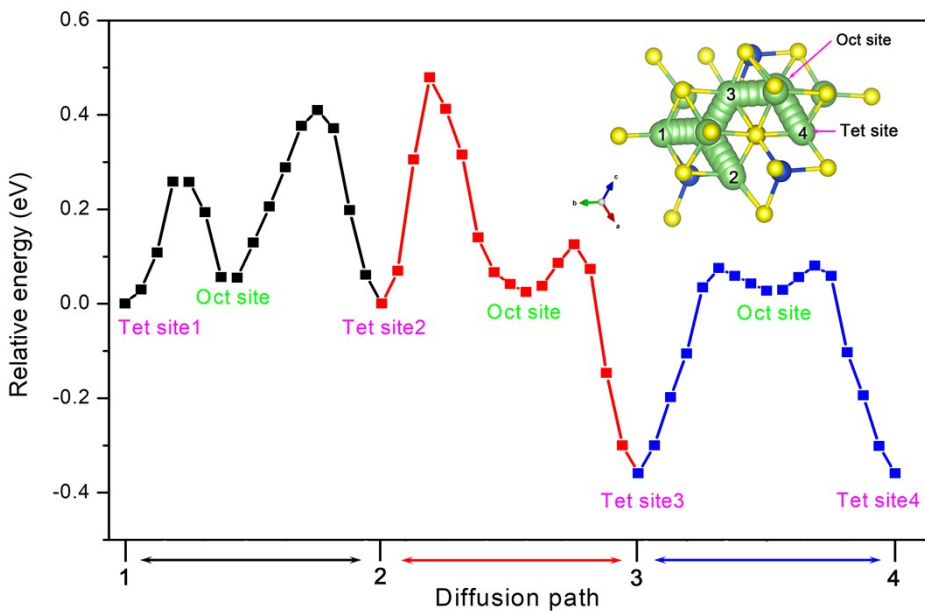


Figure S6. Energy variations of lithium ion migration by the interstitial diffusion mechanism along the path of $1 \leftrightarrow 2$, $2 \leftrightarrow 3$, and $3 \leftrightarrow 4$ from one tetrahedron site to its adjacent tetrahedron site through a transition state at the octahedron site in Li_2CuPS .

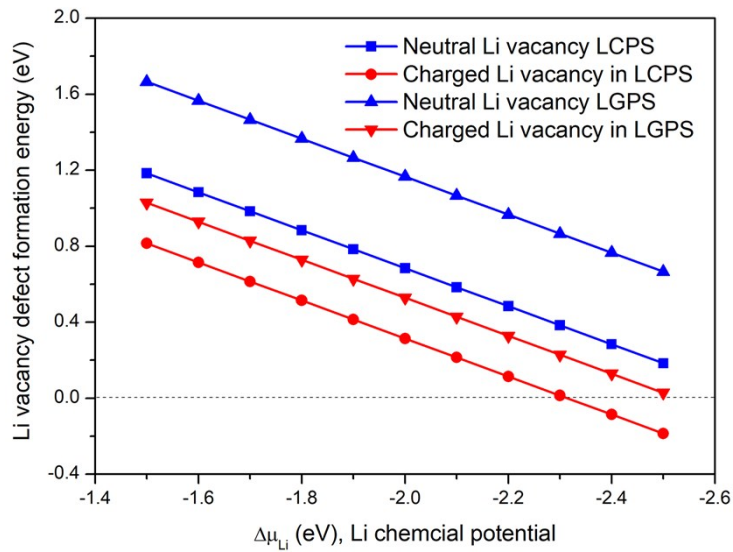


Figure S7. Neutral and charged Li vacancy defect formation energies of LCPS and LGPS as a function of Li chemical potential (eV, referred to Lithium metal). Here, both Fermi energy levels of LCPS and LGPS are set to their VBM, respectively; $\Delta\mu_{\text{Li}} = -1.50$ and -2.50 eV are the potential limits for reduction and oxidization of LCPS and LGPS, respectively.

Table S5. Atomic Bader charges (e) of the perfect and defective (a Li vacancy) LCPS $2\times 2\times 1$ supercell and LGPS $2\times 1\times 1$ supercell, respectively. Cu in LCPS lose electrons upon forming a Li vacancy, while Ge in LGPS don't do so.

LCPS			LGPS				
	perfect	defective	difference	perfect	defective	difference	
Li-1	0.884	0.884	0	Li-1	0.879	0.877	-0.002
Li-2	0.884	vacancy		Li-2	0.879	0.879	0
Li-3	0.884	0.882	0.002	Li-3	0.879	0.879	0
Li-4	0.884	0.884	0	Li-4	0.879	0.879	0
Li-5	0.884	0.884	0	Li-5	0.879	vacancy	
Li-6	0.884	0.884	0	Li-6	0.879	0.879	0
Li-7	0.884	0.884	0	Li-7	0.879	0.879	0
Li-8	0.884	0.884	0	Li-8	0.879	0.879	0
Li-9	0.864	0.865	-0.001	Li-9	0.885	0.885	-0.001
Li-10	0.864	0.865	-0.001	Li-10	0.885	0.886	0
Li-11	0.864	0.865	0	Li-11	0.879	0.879	0
Li-12	0.864	0.865	0	Li-12	0.879	0.879	-0.001
Li-13	0.864	0.865	0	Li-13	0.881	0.883	0.002
Li-14	0.864	0.865	-0.001	Li-14	0.881	0.881	0
Li-15	0.864	0.865	0	Li-15	0.881	0.881	0
Li-16	0.864	0.865	-0.001	Li-16	0.881	0.879	-0.002
Cu-1	0.489	0.516	-0.027	Li-17	0.881	0.884	0.003
Cu-2	0.489	0.516	-0.027	Li-18	0.881	0.88	0
Cu-3	0.489	0.501	-0.011	Li-19	0.881	0.88	-0.001
Cu-4	0.489	0.501	-0.011	Li-20	0.881	0.88	-0.001
Cu-5	0.489	0.501	-0.011	Ge-1	1.257	1.256	-0.001
Cu-6	0.489	0.516	-0.027	Ge-2	1.257	1.259	0.002
Cu-7	0.489	0.501	-0.011	P-1	1.244	1.239	-0.005
Cu-8	0.489	0.516	-0.027	P-2	1.244	1.251	0.007
P-1	1.182	1.177	0.005	P-3	1.272	1.269	-0.003
P-2	1.182	1.184	-0.002	P-4	1.272	1.265	-0.007
P-3	1.182	1.181	0.001	S-1	-1.029	-0.859	0.171
P-4	1.182	1.177	0.005	S-2	-1.029	-1.013	0.016
P-5	1.182	1.178	0.004	S-3	-1.029	-1.017	0.012
P-6	1.182	1.178	0.004	S-4	-1.029	-1.017	0.012
P-7	1.182	1.178	0.004	S-5	-0.96	-0.922	0.038
P-8	1.182	1.178	0.004	S-6	-0.96	-0.909	0.051
S-1	-0.855	-0.859	0.004	S-7	-0.96	-0.952	0.009
S-2	-0.855	-0.853	-0.002	S-8	-0.96	-0.943	0.017
S-3	-0.855	-0.851	-0.004	S-9	-1.005	-0.971	0.034
S-4	-0.855	-0.708	-0.147	S-10	-1.005	-1.003	0.002

S-5	-0.855	-0.708	-0.147	S-11	-1.005	-0.985	0.02
S-6	-0.855	-0.851	-0.004	S-12	-1.005	-0.991	0.014
S-7	-0.855	-0.853	-0.002	S-13	-1.192	-1.196	-0.004
S-8	-0.855	-0.859	0.004	S-14	-1.192	-1.117	0.075
S-9	-0.855	-0.851	-0.004	S-15	-1.192	-1.188	0.004
S-10	-0.855	-0.859	0.004	S-16	-1.192	-1.188	0.004
S-11	-0.855	-0.708	-0.147	S-17	-0.929	-0.919	0.01
S-12	-0.855	-0.853	-0.002	S-18	-0.929	-0.918	0.012
S-13	-0.855	-0.853	-0.002	S-19	-0.929	-0.909	0.02
S-14	-0.855	-0.708	-0.147	S-20	-0.929	-0.755	0.174
S-15	-0.855	-0.859	0.004	S-21	-1.173	-1.161	0.012
S-16	-0.855	-0.851	-0.004	S-22	-1.173	-1.167	0.006
S-17	-0.855	-0.842	-0.013	S-23	-1.173	-1.174	-0.001
S-18	-0.855	-0.843	-0.011	S-24	-1.173	-1.003	0.17
S-19	-0.855	-0.845	-0.010				
S-20	-0.855	-0.851	-0.004				
S-21	-0.855	-0.851	-0.004				
S-22	-0.855	-0.845	-0.010				
S-23	-0.855	-0.843	-0.011				
S-24	-0.855	-0.842	-0.013				
S-25	-0.855	-0.845	-0.010				
S-26	-0.855	-0.842	-0.013				
S-27	-0.855	-0.851	-0.004				
S-28	-0.855	-0.843	-0.011				
S-29	-0.855	-0.843	-0.011				
S-30	-0.855	-0.851	-0.004				
S-31	-0.855	-0.842	-0.013				
S-32	-0.855	-0.845	-0.010				

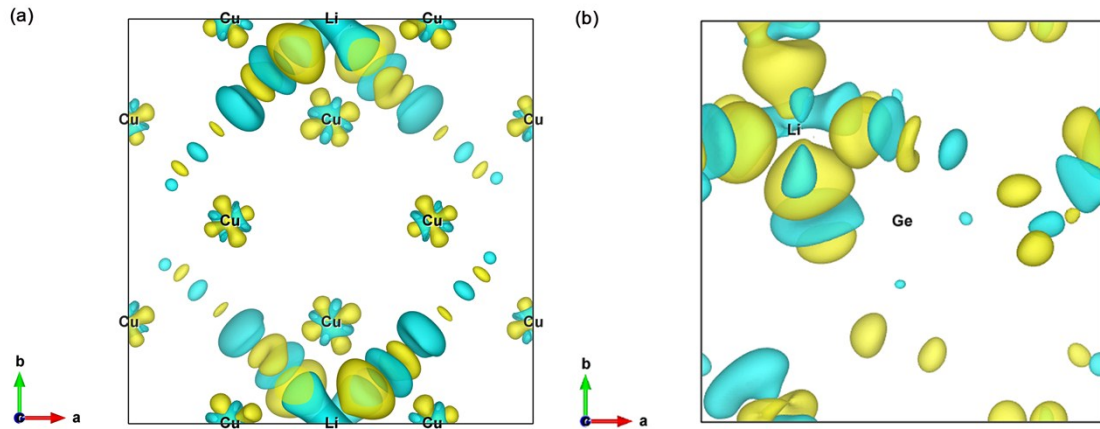


Figure S8. Charge density differences of (a) LCPS and (b) LGPS with forming a Li vacancy defect. The yellow and blue isosurfaces represent the gain or loss of electrons. Cu in LCPS loses electron when forming a Li vacancy, while Ge don't do so.

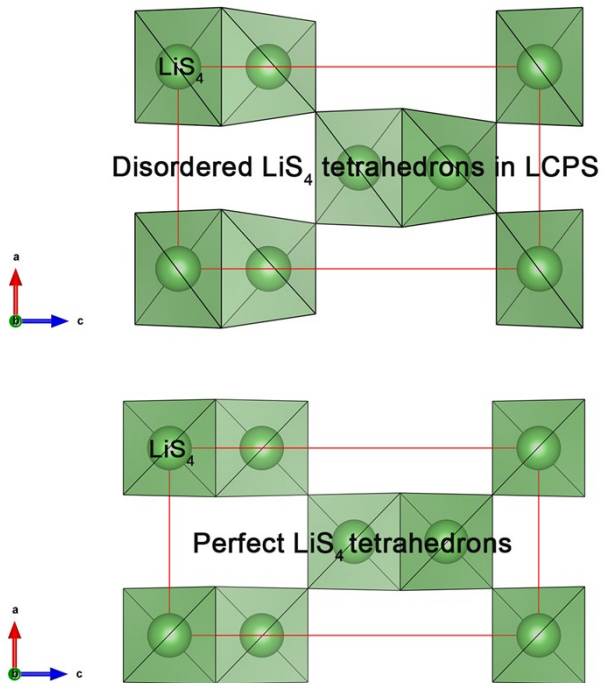


Figure S9. Disordered LiS_4 tetrahedrons in LCPS in comparison with the perfect LiS_4 tetrahedrons. Here, both the CuS_4 and PS_4 tetrahedrons are hided to highlight the LiS_4 tetrahedrons.

References

1. Z. M. Xu, S. H. Bo and H. Zhu, *ACS applied materials & interfaces*, 2018, 10, 36941-36953.
2. S. Chen, X. G. Gong, A. Walsh and S.-H. Wei, *Appl. Phys. Lett.*, 2009, 94, 041903.
3. S. L. Shang, A. Saengdeejing, Z. G. Mei, D. E. Kim, H. Zhang, S. Ganeshan, Y. Wang and Z. K. Liu, *Computational Materials Science*, 2010, 48, 813-826.
4. Y. Yang, Q. Wu, Y. Cui, Y. Chen, S. Shi, R. Z. Wang and H. Yan, *ACS applied materials & interfaces*, 2016, 8, 25229-25242.
5. A. Moradabadi and P. Kaghazchi, *Appl. Phys. Lett.*, 2016, 108, 213906.
6. S. Zhang and J. Northrup, *Phys. Rev. Lett.*, 1991, 67, 2339-2342.
7. C. Freysoldt, J. Neugebauer and C. G. Van de Walle, *Phys. Rev. Lett.*, 2009, 102, 016402.
8. K. Momma and F. Izumi, *J. Appl. Crystallogr.*, 2011, 44, 1272-1276.